
RAD4XCNN: A NEW AGNOSTIC METHOD FOR POST-HOC GLOBAL EXPLANATION OF CNN-DERIVED FEATURES BY MEANS OF RADIOMICS

Francesco Prinzi¹, Carmelo Militello^{2,*}, Calogero Zarcaro¹, Tommaso Vincenzo Bartolotta¹, Salvatore Gaglio^{3,2}, and Salvatore Vitabile¹

¹Department of Biomedicine, Neuroscience and Advanced Diagnostics, University of Palermo, Palermo, 90127, Italy

²Institute for High-Performance Computing and Networking (ICAR-CNR), National Research Council, Palermo, 90146, Italy

³Department of Engineering, University of Palermo, Palermo, 90128, Italy

*Corresponding author: email: carmelo.militello@cnr.it

April 26, 2024

ABSTRACT

In the last years, artificial intelligence (AI) in clinical decision support systems (CDSS) played a key role in harnessing machine learning and deep learning architectures. Despite their promising capabilities, the lack of transparency and explainability of AI models poses significant challenges, particularly in medical contexts where reliability is a mandatory aspect. Achieving transparency without compromising predictive accuracy remains a key challenge. This paper presents a novel method, namely Rad4XCNN, to enhance the predictive power of CNN-derived features with the interpretability inherent in radiomic features. Rad4XCNN diverges from conventional methods based on saliency map, by associating intelligible meaning to CNN-derived features by means of Radiomics, offering new perspectives on explanation methods beyond visualization maps. Using a breast cancer classification task as a case study, we evaluated Rad4XCNN on ultrasound imaging datasets, including an online dataset and two in-house datasets for internal and external validation. Some key results are: *i*) CNN-derived features guarantee more robust accuracy when compared against ViT-derived and radiomic features; *ii*) conventional visualization map methods for explanation present several pitfalls; *iii*) Rad4XCNN does not sacrifice model accuracy for their explainability; *iv*) Rad4XCNN provides global explanation insights enabling the physician to analyze the model outputs and findings. In addition, we highlight the importance of integrating interpretability into AI models for enhanced trust and adoption in clinical practice, emphasizing how our method can mitigate some concerns related to explainable AI methods.

Keywords Explainable AI · Radiomics · Convolutional Neural Networks · Breast Cancer · Clinical Decision Support Systems

1 Introduction

The use of computer-aided tools based on Artificial Intelligence (AI) methods has increased significantly. These tools utilize machine learning and deep learning architectures in many types of Decision Support Systems (DSS). A particular class of DSS is represented by Clinical decision support systems (CDSS), implemented to support activities in critical healthcare processes. Although data-driven methods play a crucial role in CDSSs development, their use in medicine still harbors many pitfalls. New deep learning methods and the growing data availability have enabled the development of powerful but uninterpretable CDSS, and the field of Explainable AI (XAI) has gained considerable attention. Regulatory authorities have addressed the problem of explainability Kundu [2021], Arrieta et al. [2020].

The US Federal Trade Commission emphasizes that AI tools should be transparent, explainable, fair, and empirically based while promoting accountability Smith and Director [2020]. The European Parliament has adopted the General Data Protection Regulation (GDPR), in which meaningful explanations of the logic involved are declared mandatory when automated decision-making is performed Guidotti et al. [2018]. The lack of transparency makes both doctors and patients skeptical about these new technologies. Opaque AI systems can impair the doctor-patient relationship and jeopardize patient trust Amann et al. [2020]. For this reason, scientific research is working on making AI transparent and/or explainable Combi et al. [2022]. In medical contexts, several aspects can affect the model reliability and demand explainability Holzinger [2016], Holzinger et al. [2019]. Consequently, methods that enable transparency and explainability can help validate the models, improve the knowledge domain, and increase the real-world usability of the systems.

For these reasons, although it is not yet fully accepted Bornstein [2016], Ghassemi et al. [2021], McCoy et al. [2022], London [2019], explainability is increasingly becoming a requirement that these systems should fulfill Jovanović and Schmitz [2022].

Deep learning architectures have demonstrated remarkable capabilities in extracting intricate patterns and features from huge datasets, enabling unprecedented predictive performance in various fields, including medical image analysis. Although deep features achieve impressive accuracy, they ignore the question of explainability and several approaches were proposed for their *post-hoc* explanation. These approaches focus mainly on the concept of visualization maps that have shown several limitations regarding their reliability Cerekci et al. [2024], Prinzi et al. [2024a], Zhang et al. [2021].

Radiomics Gillies et al. [2016], Lambin et al. [2017] is a new alternative approach to introduce explainability within the feature extraction process in medical imaging Prinzi et al. [2024b]. In Radiomic, features are calculated by appropriate mathematical formulas applied to the greyscale histogram, to texture-defining matrices or ROIs shape quantifiers. As a result, the meaning of each radiomic feature is well known and meaningful clinical conclusions can be drawn through model explanation Prinzi et al. [2024c].

Although radiomic features have the great property of inherent explainability, their predictive power seems considerably weaker than deep features, as has been shown in several works Lisson et al. [2022], Sun et al. [2020], Truhn et al. [2019], Wei [2021]. Again, the dilemma concerning the trade-off between explainability and accuracy arises. Hence, the use of deep features would ensure highly performing but poorly interpretable models, in contrast, radiomic features would ensure less accurate but explainable models.

In this study, we attempt to combine the predictive power of deep features with the intrinsic explainability characteristic of radiomic features. To this aim, state-of-the-art architectures such as ResNet, DenseNet, and Vision Transformer (ViT) for deep feature extraction were employed. Simultaneously, a radiomic workflow to extract interpretable signatures was implemented. We performed a comparative analysis between these two feature sources in terms of predictive performance and explainability. Moreover, the new method Rad4XCNN proposed in this work combines the predictive power of the deep features while exploiting the inherent interpretability of the radiomic features. In particular, Rad4XCNN doesn't introduce constraints or bottlenecks that can harm accuracies in deep architecture training while explaining CNN-derived features by means of radiomics. In addition, it provides new perspectives on the development of explanation methods not solely relying on visualization maps Papanastasiou et al. [2023]. A breast cancer classification task was proposed as a case study to evaluate the effectiveness of Rad4XCNN: this application reflects the challenges encountered in real-world clinical scenarios. To this end, we acquired two in-house datasets, one for training and internal testing and the other for external validation.

The main contributions are:

- Rad4XCNN a new method able to explain deep features by means of radiomics;
- a comparison between deep and radiomic features in terms of explainability and accuracy, providing insights on the importance of proposing new methods to overcome the accuracy-explainability trade-off dilemma;
- the use of deep architectures for breast cancer classification in ultrasound (US) imaging exploiting an online dataset, and two in-house datasets for internal and external tests;

The rest of the article is structured as follows: Section 2 'Background' Section introduces the main concepts of explainable AI and focuses on methods for explaining deep architectures and radiomic models. Section 3 'Materials and Methods' describes the datasets and the methods implemented, including our novel approach for global explanation of deep features. Section 4 'Experimental Results' compares the results of deep architectures and radiomic models in terms of accuracy and explainability. Section 5 'Discussion' Section exposes the importance of our approach to obtain accurate and interpretable models. Finally, Section 6 'Conclusion' highlights the main results.

2 Background

Explainable AI Numerous definitions of explainable AI are not fully standardized yet Longo et al. [2024]. For this article, it is essential to delineate certain concepts. A model is *intrinsically interpretable* when its transparent structure allows an understanding of its decision process. For this reason, a transparent algorithm doesn't require explanation methods for its interpretation. From an algorithmic point of view, Logistic Regression, Decision Tree, and Naive Bayes are transparent. Neural Networks (NNs), Support Vector Machines (SVMs), and Tree Ensemble (TE) are defined as *black-boxes* and require explanation methods for their introspection. An explanation can be global and local. A *global explanation* aims to explain a model's behavior across its entire dataset. A *local explanation* aims to explain the prediction of a specific dataset sample (i.e. patient). To an *intelligible feature* it is possible to associate a human-understandable meaning. Radiomic features are considered intelligible. Conversely, *deep features* (e.g. extracted via neural network architectures) are not intelligible. We can call features extracted via convolutional neural networks *CNN-derived*, and extracted via Vision Transformer as *ViT-derived*.

The combination of intelligible features and transparent algorithms makes the whole system intrinsically interpretable for two reasons: 1) it is possible to calculate the impact of the feature for model decision; 2) it is possible to correlate and validate the model's findings comparing it with the clinical literature. When black-box algorithms are used and the features are intelligible, explanation methods allow for global and local explanations. Typically, these methods are called *post-hoc algorithms* because they are applied after model training. Model explainability becomes much more complicated when not-intelligible features are used: model findings cannot be correlated with clinical literature because the meaning of each feature is unknown (as happens with learned features in deep architectures). A method is defined *agnostic* when can be applied to any algorithm and architecture. For classification tasks, an XAI method can be *class-dependent* when explanations are given for each class separately, conversely, they are defined as *class-independent*.

Explainability in Deep Architectures Convolutional-based neural networks have emerged as a standard for deep feature extraction in medical images. The explainability of these architectures is mainly focused on the concept of saliency maps, implemented to highlight the image areas most informative for the prediction Itti et al. [1998], Mamalakis et al. [2023]. In Simonyan et al. [2013] the gradient computation of the class score concerning the input image is exploited to visualize the activation map specific to a given image and a particular class. Integrated gradients are proposed in Sundararajan et al. [2017] for a more robust explanation through activation maps, adding the constraint of respecting the '*sensitivity*' and the '*implementation invariance*' principles/axioms. In Zeiler et al. [2011] and Zeiler and Fergus [2014] a network using deconvolution is proposed to visualize the convolutional network and in Springenberg et al. [2014] a variant of the deconvolution approach with guided back-propagation is proposed to visualize the features learned from CNN. The most popular algorithms exploiting saliency belong to the category of 'class activation maps' (CAM) Zhou et al. [2016]. GradCAM Selvaraju et al. [2017] has been introduced after CAM, to overcome the limitation of being able to visualize only the last layer and only particular CNN architectures. Despite many other methods being proposed later, GradCAM remains one of the most widely used. Lately, methods called 'gradient-free' are also gaining wide popularity to overcome some limitations for computing gradients in very-deep architectures, and overcome the problem of anomalous behavior in incorrect prediction scenarios Muhammad and Yeasin [2020].

Saliency maps are mainly used to provide local explanations and it is not clear how these tools can be used for global explanation. Furthermore, it is important to emphasize that criticisms have been raised about their use Prinzi et al. [2023a]. For example, poorly localized, and spatially blurred visualization was found in some cases Oh et al. [2020], Signoroni et al. [2021]. Moreover, it has been shown that different saliency map computation techniques can produce conflicting results Prinzi et al. [2024a], Zhang et al. [2021].

Radiomic Workflow Radiomics is gaining prominence for extracting features from radiological images. It operates on the premise that some pixel-wise patterns are hidden from the human eye. For this reason, it is defined as a workflow aimed to convert standard-of-care medical images into high-dimensional data Gillies et al. [2016]. In contrast to deep features, radiomic features are computed through mathematical formulas applied to the images and quantify some characteristics such as texture/pattern and statistical measurement. For this reason, radiomic features are also called *hand-crafted*, counterposed to the *learned* extracted by neural networks. Radiomic flow has several advantages over deep extraction. While deep extraction requires large datasets for model training, radiomic feature extraction can be performed with small datasets Wei [2021]. Moreover, shallow learning algorithms prove to be well-suited for classifying radiomic data, widely recognized as more appropriate for training with small datasets. The main advantage lies in the inherent interpretability of radiomic features Militello et al. [2023], Prinzi et al. [2024b]: it is well known the meaning each feature expresses. The use of shallow learning algorithms and intrinsically interpretable features enables the local and global introspection of the predictive models.

Our Rationale Despite in some applications the use of transparent models can be sufficient Rudin [2019], the design of a transparent model can introduce a level of complexity Chen et al. [2022]: interpretable features are typically less informative than deep features. In addition, the use of transparent algorithms may fail when the relationships between the data are complex and nonlinear. As a consequence, the use of transparent-by-design models can lead to poor performance. For this reason, the eternal conflict between the explainability and accuracy trade-off comes into play.

The literature indicates the need for new methods that deviate from those based on visualization maps Papanastasiou et al. [2023]. Some attempts have been made by Paul et al. [2019], Wang et al. [2019], Chen et al. [2016] although there is no explicit reference to XAI. Paul et al. [2019] evaluated how radiomic model performance varies by replacing a correlated deep feature in the radiomic signature. However, regarding the performed interpretable feature extraction, the Image Biomarkers Standardization Initiative (IBSI) guidelines Zwanenburg et al. [2020] had not yet been proposed at that time. As a consequence, assessing the reproducibility of the study and the resulting impact of the study can be challenging. In addition, the authors do not use state-of-the-art deep extraction architectures such as ResNet, DenseNet, and ViT, whose depth is quite different from the VGG employed. Furthermore, they agree with an important limitation regarding the fact that a single slice was used to extract deep features in a volumetric image, whereas semantic information was generated from multiple slices. Above all, in contrast to our idea, they modify the input signature by replacing semantic features with deep ones, introducing a kind of constraint for model training. Wang et al. [2019] attempts to exploit the radiologist’s knowledge to qualitatively and visually correlate CNN-based feature maps with semantic features related to the investigated domain. However, these radiological features are operator-dependent, as is their correlation with the feature maps. As a result, their proof-of-concept is not generalizable to any context or domain. A similar idea was proposed in Chen et al. [2016], to effectively bridge the gap between deep features and multiple clinical semantic features. The model aims to yield semantic rating scores to support a deeper analysis for either clinical diagnosis or educational purposes. More recently, Liu et al. [2023] tried to train deep models to grade informative semantic features related to the analyzed task rather than directly predicting the disease malignancy. Both papers lack formalism regarding the terminology related to explainable AI (i.e., the characteristics of the method in terms of global-local explanation, applicability, class dependencies, etc.) In general, in the attempt to make the predictive process transparent, the cited articles, employ semantic features subject to inter-operator variability or modify the training process, which could harm the established predictive performance of deep models.

In this paper, we present Rad4XCNN, a method that integrates the predictive strengths of deep features with the interpretability offered by radiomic features. The method does not introduce any constraints in the training that inhibit its accuracy. Considering the development of new explanation methods not solely based on visualization maps as a major challenge Papanastasiou et al. [2023], Rad4XCNN offers an innovative approach to explain deep architectures and provides a global explanation of deep networks, an aspect often overlooked in current research.

3 Materials and Methods

Figure 1 shows the flow diagram of the proposed method. For the deep workflow ResNet50, DenseNet121, and ViT-B32 were pre-trained on the BUSI dataset. Then the extracted deep features were employed both for classification (via multilayer perception) and for explanation (local explanation via visualization maps). For the radiomic workflow, radiomic features were extracted, preprocessed, and used to train shallow classifiers. Radiomic and deep features were used as input for Rad4XCNN providing a global explanation.

3.1 Datasets Description

Breast Ultrasound Images Dataset (BUSI) The Breast Ultrasound Images Dataset (BUSI) Al-Dhabyani et al. [2020] comprises 780 US images obtained from 600 patients aged 25-75 years in 2018, alongside corresponding masks in PNG format. The images - containing the Focal Breast Lesions (FBLs) - measure around 500×500 pixels. They are categorized into three classes: benign, malignant, and normal. Among these, 437 images present benign lesions, 210 are malignant, and 133 are classified as normal. Normal samples were not used in the study. The dataset exhibits class imbalance, with 67.49% benign samples and 32.51% malignant.

Palermo and Cefalù Datasets Two *in-house* datasets were collected on two centers, referred to as *Palermo* and *Cefalù* datasets. Considering the Palermo site, 237 breast cancer patients were enrolled in 2021 at Policlinico Universitario “P. Giaccone”. The obtained dataset was split into two subsets (with an 80/20 ratio) used for the training and testing phases, respectively. Instead, considering the Cefalù site, 115 breast cancer patients were enrolled in 2022 at Fondazione Istituto “G. Giglio” Breast Unit. This dataset was used for model external validation. Table 1 provides a detailed explanation of the in-house datasets.

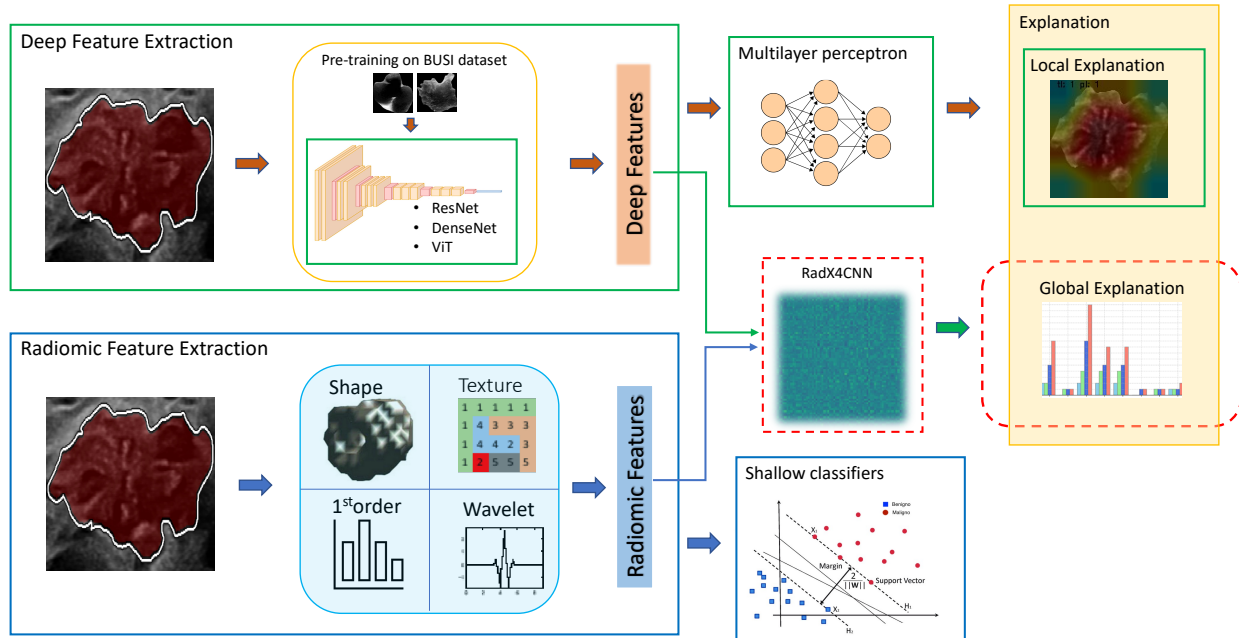


Figure 1: Overall workflow. Deep and Radiomic approaches were implemented for feature extraction and classification. Successively, radiomic and deep features were employed for Rad4XCNN implementation, providing a global explanation method.

Table 1: Description of the in-house collected dataset, coming from Palermo and Cefalù hospitals.

Characteristic	Palermo Dataset	Cefalù Dataset
image size	845×600	845×600
focal breast lesions	237	115
benign lesion	132	70
malignant lesion	105	45
size range [mm]	4-90	3-50
mean size [mm]	15.12 ± 9.44	14.64 ± 8.61
age range [years]	17-88	23-89
mean age [years]	53.15 ± 15.00	51.61 ± 14.56

FBL images of both datasets were acquired through the B-mode US modality. In particular, two experienced breast radiologists (one for each center, more than 30 years of experience in breast imaging) performed US acquisition through two identical ultrasound RS85 (manufactured by Samsung Medison, Co. Ltd.) units, each provided with the same 3–12 MHz linear transducer. Acquired FBLs were labeled according to US BI-RADS criteria Sickles and D’Orsi [2014] by expert radiologists and successively segmented.

In both centers, indications for breast US included:

- a palpable mass detected on physical examination;
- dense breasts;
- detected lesions from adjunct mammography examination;
- patients with mastodynia;
- young patients having a family history
- patients in a follow-up for benign breast nodules

Patients have not undergone any intervention or surgery on lesions before US examination. Exclusion criteria included lack of adequate standard of reference (refusal to undergo biopsy or inconsistent follow-up).

3.2 Deep Architecture Training

This section includes the workflow description to train deep architectures. In particular, preprocessing strategies, data preparation for training and test, and the implemented architectures are discussed. In addition, state-of-the-art methods for deep features explanation were exposed as well as our novel Rad4XCNN method.

Image preprocessing Patches were extracted from the whole image using the available masks. All patches were resized to size 128×128 , specifically: *i*) images with a size larger than 128×128 were subsampled, and *ii*) zero-padding was applied to images with a smaller size. Images were normalized before model training.

Training and test protocol The BUSI dataset was divided into training and test sets, using the ratio 80:20. The training set was split again into training and validation sets, with the same ratio. In addition, the training set was balanced by considering random flip, rotation, contrast enhancement, translation, and zoom. Considering the recent criticism about the BUSI dataset Pawłowska et al. [2023], it was used only to obtain an optimized pre-trained model. Regarding the Palermo in-house dataset, 15% was used as an independent test set, while the remaining 85% was used to implement a 5-fold cross-validation (CV). The Cefalù dataset was used only for external testing. The best model in terms of accuracy within the CV procedure was selected for the Palermo internal test and the Cefalù external test.

Regarding the architectures, state-of-the-art models were employed, including Densenet121, Resnet50, and ViT-B32. The extracted feature vector in ResNet50 and DenseNet121 is 2048 and 1024 neurons, respectively. Their head was implemented using (1) a dropout layer, (2) a dense layer with 512 neurons, (3) another dropout, and (4) the last dense layer with 2 neurons. Regarding ViT-B32, the extracted feature vector was 768 dimensions, followed by (1) a dropout layer, (2) a batch normalization layer, and (3) two dense layers of 512 and 2 neurons, respectively. The softmax activation function was used on the last dense layer and the ReLU for the others.

Saliency Maps Computation Saliency maps highlight regions of an input image that most contribute to the prediction. Considering a classification task with c classes and a convolutional neural network with A^k feature map activations, Grad-CAM Selvaraju et al. [2017] is formalized as:

$$L_{Grad-CAM}^c = ReLU\left(\sum_k \alpha_k^c A_l^k\right) \quad (1)$$

where:

$$\alpha_k^c = \frac{1}{z} \sum_i \sum_j \frac{\partial y^c}{\partial A_{ij}^k} \quad (2)$$

Here $\frac{1}{z} \sum_i \sum_j$ represents the global average pooling operator over the width and height dimensions (indexed by i and j respectively) and $\frac{\partial y^c}{\partial A_{ij}^k}$ gradients via backpropagation. The weights α_k^c represent a partial linearization capture the importance of feature map k for a target class c . Grad-CAM’s dependence on class c makes it a class discriminative method. Although Grad-CAM appears as one of the most widely used approaches, has two main limitations related to the gradient computation: *i*) saturation: Gradient can vanish due to the saturation problem for Sigmoid function or the zero-gradient region of ReLU function; and *ii*) false confidence: Activation maps with higher weights show lower contributions to the network’s output compared to a zero baseline Wang et al. [2020]. In addition, backpropagating any quantity requires additional computational overhead and assumes that classifiers produced correct decisions, and whenever a wrong decision is made, all mentioned methods will produce wrong or distorted visualizations Muhammad and Yeasin [2020].

In contrast to Grad-CAM Selvaraju et al. [2017], which use the gradient information flowing into the last convolutional layer to represent the importance of each activation map, the Channel-wise Increase of Confidence (CIC) was introduced in Score-CAM Wang et al. [2020].

$$L_{Score-CAM}^c = ReLU\left(\sum_k \alpha_k^c A_l^k\right) \quad (3)$$

with:

$$\alpha_k^c = C(A_l^k) \quad (4)$$

where $C(\cdot)$ denotes the Channel-wise Increase of Confidence (CIC) defined to measure the importance of each activation map.

EigenCAM is a gradient-free method and uses the principal components from the extracted feature maps Muhammad and Yeasin [2020]. For this reason, it can overcome the problem of distorted displays in case of incorrect predictions. Let I represent the input image of size $(i \times j)$, $I \in \mathbb{R}^{i \times j}$, and let $W_{L=k}$ represent the combined weight matrix of the first k layers of size (m, n) . The class activated output is the image I projected onto the last convolution layer $L = k$ and is given by $O_{L=k} = W_{L=k}^T I$, factorizing $O_{L=k}$ using singular value decomposition to compute the principal components of $O_{L=k}$ gives $O_{L=K} = U \Sigma V^T$. U is a $M \times M$ orthogonal matrix and the column U are the left singular vectors, Σ is a diagonal matrix of size $M \times N$ with singular values along the diagonal and V are the left singular vectors. The class activation map, $L_{EigenCAM}$ is given by the projection of $O_{L=k}$ on the first eigenvector:

$$L_{EigenCAM} = O_{L=K} V_1 \quad (5)$$

where V_1 is the first eigenvector in the V matrix. Eigen-CAM is class-independent, e.g. the result of saliency maps is not tied to any class.

3.3 Radiomic Models Training

Radiomic workflow includes ROI segmentation, feature extraction, feature preprocessing, selection, and model training.

ROI Segmentation ROI segmentation was performed by radiologists from each B-mode image of the breast lesion through S-Detect™. This software is commercially available, licensed for clinical use, and installed on the RS85 ultrasound unit.

Feature Extraction A total of 474 radiomic features were extracted using PyRadiomics Van Griethuysen et al. [2017], a toolkit compliant with the IBSI Zwanenburg et al. [2020]. IBSI aims to standardize the radiomic analysis process, improving workflow reproducibility. Extracted features belong to the following categories: shape 2D; first-order intensity histogram statistics; Gray Level Co-occurrence Matrix features (GLCM); Gray Level Run Length Matrix (GLRLM); Gray Level Size Zone Matrix (GLSZM); Gray Level Dependence Matrix (GLDM); Neighboring Gray Tone Difference Matrix (NGTDM). Features were extracted discretizing images to 255 gray levels. In addition, considering the predictive capability of wavelet-derived radiomic features compared to the original ones Prinzi et al. [2023b], non-shape features were extracted also considering the Haar wavelet transform.

Features Preprocessing and Selection Non-redundant and informative features were selected Militello et al. [2022], Papanikolaou et al. [2020] through: *i*) near-zero variance analysis to remove features with low information content (variance cutoff $\sigma^2 = 0.005$); *ii*) correlation analysis to remove highly correlated features (the Spearman correlation with a 0.9 threshold value was considered). The Sequential Feature Selector (SFS) algorithm combined with XGBoost (XGB), Random Forest (RF), and SVM classifiers was used to select the most discriminating features. Accuracy was used as a metric to maximize.

Predictive Model Setup This study employed three distinct shallow classifiers: RF, XGB, and SVM. These algorithms have proven suitable for tabular data in small dataset scenarios Prinzi et al. [2022]. RF and XGB were trained using 100 estimators. For XGB a learning rate of 0.3 and gain as the importance type were employed. SVM training involved standardizing the features and RBF kernel. The predictive model setup was performed on the training set using the XGB classifier and considering a stratified 10-fold Cross-Validation procedure repeated 20 times. The best model in terms of accuracy found during the 20-repeated 10-fold cross-validation procedure was selected for the test.

3.4 Deep Features Explanation by means of Radiomics

Rad4XCNN aims to explain the deep features extracted through the intrinsic meaning of radiometric features. Let $f_r = (r_1, r_2, \dots, r_a)$ denote the radiomic features, and $f_d = (d_1, d_2, \dots, d_b)$ denote the deep features, where a and b are the number of radiomic and deep features, respectively. The method assumes the use of a correlation index, and Spearman's test was employed in this work. The Spearman correlation coefficient between f_r and f_d is given by:

$$\rho_{i,j} = \frac{\text{cov}(r_i, d_j)}{\sigma_r \sigma_d} \forall i \in [1, a], j \in [1, b], \text{ with } i, j \in \mathbb{N} \quad (6)$$

where: $\text{cov}(r_i, d_j)$ is the covariance between r_i and d_j , σ_r is the standard deviation of r_i , σ_d is the standard deviation of d_j .

To explain the meaning of f_d exploiting the correlation with the features f_r using a thresholds M , a threshold function $T(\rho, M)$ is defined such that:

$$T(\rho, M) = \begin{cases} 1 & \text{if } \rho \geq M \\ 0 & \text{otherwise} \end{cases} \quad (7)$$

where: ρ is the Spearman correlation coefficient between f_r and f_d , M is the threshold value. M represents a method hyperparameter to be determined according to the specific case study. By applying different threshold values, it is possible to determine which features in f_d are correlated with radiomic features f_r . It assumed that correlated radiomic and deep features describe the same phenomenon (e.g. features have a similar meaning) Paul et al. [2019], Wang et al. [2019]. Below are the main characteristics of the proposed method:

Global Explanation Our method implements the notion of global explanation, diverging from approaches reliant on computing saliency maps, which constitute a form of local explanation. Global explanation is a key aspect of clinical model validation as it facilitates a comparative analysis of model findings against the existing clinical literature.

Model-agnostic This method is agnostic, making it universally applicable across architectures and application contexts. It merely necessitates the extraction of feature vectors f_d and f_r , rendering it adaptable to any model and application without constraints. In agreement with the other saliency maps methods, Rad4XCNN need the vectorized version f_d of features maps A_{ij}^k , such as Grad-CAM, Score-CAM and $W_{L=k}$ Eigen-CAM.

Class-Independent Rad4XCNN explains deep features without class specificity, such as Eigen-CAM. Conversely, it contrasts with Grad-CAM and Score-CAM, which are class-dependent considering the computation of α_k^c .

Ease of Implementation It requires only the extraction of f_d , which is inherently part of any training process, along with the extraction of radiomic features f_r and the subsequent calculation of their correlation. The simplicity of implementation is the basis of several widely adopted and popular techniques Muhammad and Yeasin [2020], Zeiler and Fergus [2014].

4 Experimental Results

Deep models were trained using Adam optimizer and 8 as batch size. For ResNet50 and DenseNet121 10^{-4} was used as the learning rate, and 10^{-5} for ViT. A rate of 0.5 was used for dropout layers. The BUSI dataset was employed to obtain an initial pre-trained model, and 80% of the Palermo dataset was used for fine-tuning. Then, the remaining 20% of the Palermo dataset was used as an internal test and the whole Cefalù dataset for an external test.

4.1 Deep and Radiomic Models Performance

Table 2 provides a comparison between radiomic and deep models considering the Palermo training dataset. ResNet50, DenseNet121, and ViT-B32, demonstrate remarkable performance compared to radiomic models. ResNet achieves an impressive accuracy of $93.62\% \pm 9.19$ and AUROC of 0.95 ± 0.09 , showcasing its robustness in classification tasks. Similarly, DenseNet and ViT exhibit high accuracies and AUROC scores, proving the dominance of deep learning-based approaches over radiomic models. In contrast, models incorporating radiomic features coupled with traditional machine learning algorithms such as XGB, RF, and SVM perform poorly compared to deep architectures.

Internal and external test performance are shown in Table 3, in which again the superiority of deep models over radiomic-based approaches is shown. In the Palermo dataset, ResNet achieves an accuracy of 72.22% and AUROC of 0.733, while DenseNet and ViT achieve even higher accuracies and AUROC scores. These results highlight the effectiveness of deep learning methodologies in extracting meaningful features from the datasets, leading to improved diagnostic performance. On the Cefalù dataset, a similar trend is observed, with deep models outperforming radiomic-based approaches. In particular, ResNet proved the best generalization capability on the external test, showing an accuracy of 73.04% and a good balance between sensitivity and specificity. It is important to emphasize that although

the performance of ResNet on the internal test is much lower than ViT, on the external test ResNet maintains its performance, as opposed to ViT which achieves a heavy degradation. For this reason, we consider ResNet the best trained model, and further considerations on explainability are provided for ResNet.

In contrast, models incorporating radiomic features combined with traditional machine learning algorithms consistently demonstrate inferior performance compared to deep learning models on both internal and external test datasets. These results underscore the limitations of radiomic-based approaches in capturing complex patterns and features present in medical images, particularly when compared to the feature extraction capabilities of deep learning architectures.

Table 2: Cross-validation performance comparison of VGG, ResNet, ViT, and the radiomic model on the Palermo training dataset.

Model	Accuracy	AUROC	Sens	Spec	PPV	NPV
ResNet50	93.62 ± 9.19	0.95 ± 0.09	91.20 ± 14.83	96.26 ± 4.6	95.23 ± 5.91	93.01 ± 12.00
DenseNet121	93.17 ± 13.66	0.94 ± 0.12	93.33 ± 13.33	93.00 ± 14.00	93.33 ± 13.33	93.00 ± 14.00
ViT-B32	93.65 ± 11.5	0.97 ± 0.6	92.16 ± 12.95	95.00 ± 10.00	94.74 ± 10.53	92.80 ± 12.42
Rad + XGB	61.49 ± 9.88	0.65 ± 0.10	53.63 ± 16.79	67.53 ± 14.13	56.63 ± 13.19	66.05 ± 9.59
Rad + RF	59.93 ± 9.19	0.60 ± 0.11	39.61 ± 14.31	75.35 ± 13.01	56.66 ± 17.76	62.10 ± 7.34
Rad + SVM	65.05 ± 8.31	0.62 ± 0.10	55.83 ± 15.05	72.09 ± 12.13	61.52 ± 10.06	68.70 ± 8.60

Table 3: Internal and external test performance using ResNet, DenseNet, ViT, and radiomic models on the Palermo and Cefalù test datasets.

Model	Palermo Dataset						Cefalù Dataset					
	Acc	AUROC	Sens	Spec	PPV	NPV	Acc	AUROC	Sens	Spec	PPV	NPV
ResNet50	72.22	0.733	66.67	76.19	66.67	76.19	73.04	0.757	77.78	70.00	62.5	83.05
DenseNet121	77.78	0.784	73.33	80.95	73.33	80.95	70.44	0.755	68.89	71.43	60.78	78.13
ViT-B32	83.33	0.848	93.33	76.19	73.68	94.12	62.61	0.742	77.78	52.86	51.47	78.72
Rad + XGB	47.22	0.43	46.15	47.82	33.33	47.22	61.11	0.60	60.86	61.35	62.89	60.86
Rad + RF	58.33	0.61	61.15	56.52	44.44	58.33	51.12	0.55	54.78	53.47	56.25	54.78
Rad + SVM	58.33	0.58	53.84	60.86	43.75	58.33	58.17	0.62	58.26	58.08	60.09	58.26

4.2 Traditional CNN Explainability

As the most accurate model in the external test, ResNet was selected to analyze the traditional explainability methods based on saliency maps. By comparing the saliency maps obtained with GradCAM, EigenCAM, and ScoreCAM methods, it is possible to observe conflicting results among these interpretability techniques. Figure 2 shows some examples. Despite ResNet’s robust performance, the interpretations provided by these methods often diverged, presenting a challenge in understanding the model decision. This discrepancy raises questions about the reliability and consistency of these interpretability methods, urging a closer examination of their underlying mechanisms. Similar inconsistencies are recently achieved in Cerekci et al. [2024], Zhang et al. [2021]. In particular, rows 1-2 show two examples of correctly classified lesions, while Rows 3-4 show two examples of wrongly classified lesions. Some explanations predominantly focused on background regions, even when the model’s prediction was correct. Other concerns arise in the case of wrong prediction. Considering Grad-CAM, this effect is due to the dependence of the gradient calculation of $\frac{\partial y^c}{\partial A_{ij}^k}$ (see Equation 2) that is a function of the prediction y^c , assumed correctly predicted the class c . For Score-CAM this problem is mitigated by CIC which weights the importance of each activation map. For Eigen-CAM decomposition does not depend on the predicted class and gradient computation. This phenomenon underlines the complexity of interpreting neural network decisions and highlights the need for newer interpretability techniques capable of overcoming these problems and providing clearer and more actionable insights.

4.3 Explaining Deep Features by means of Radiomics in US Breast Dataset

Figure 3 depicts the Rad4XCNN results, utilizing four distinct threshold values $\rho = [0.30, 0.35, 0.40, 0.45]$. Notably, the graph exclusively illustrates correlations with deep features derived from convolutional networks, as no correlations

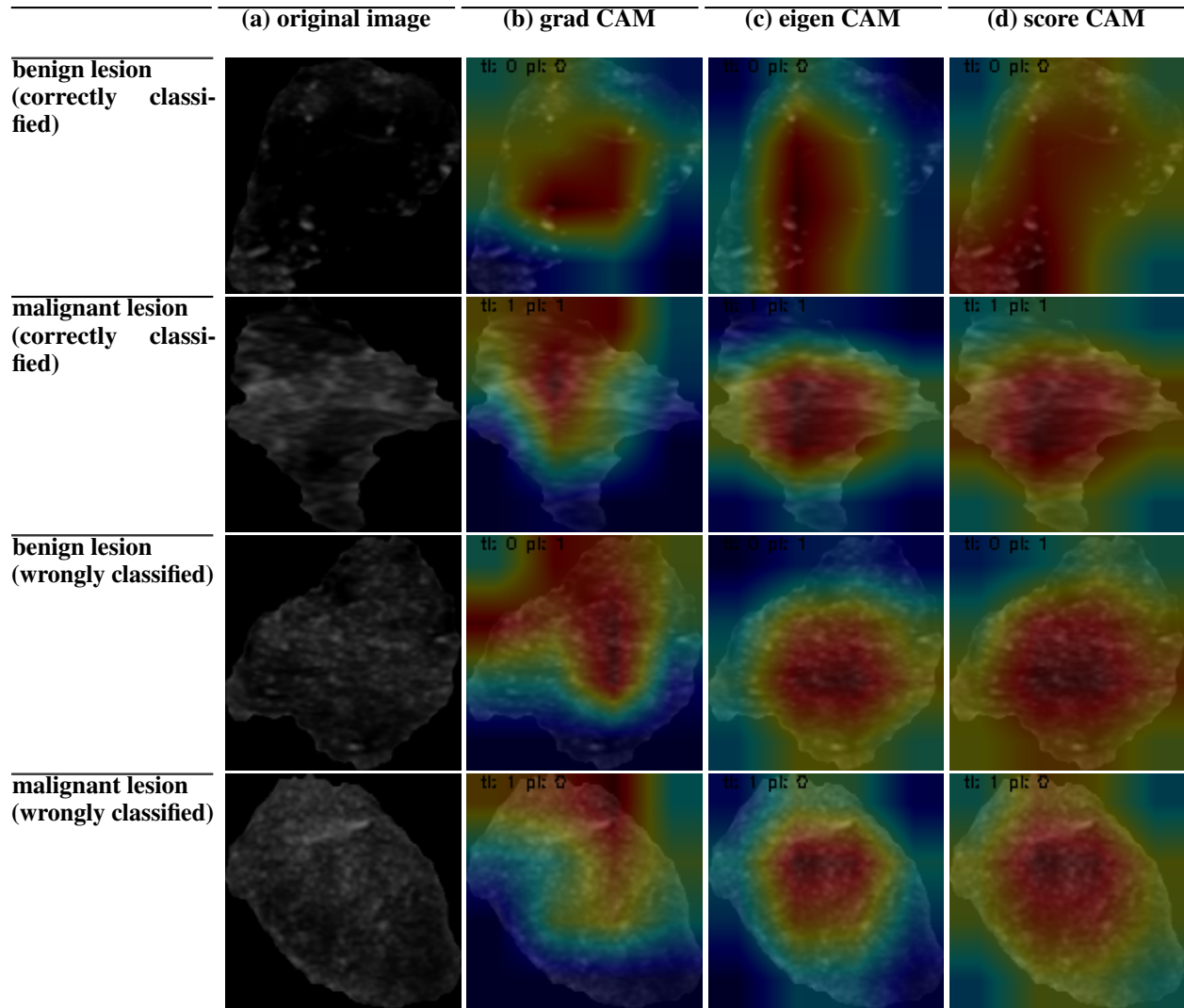


Figure 2: (a) original ultrasound image; (b) ultrasound image with overlapped the grad CAM saliency map; (c) ultrasound image with overlapped the eigen CAM saliency map; (d) ultrasound image with overlapped the score CAM saliency map.

were identified with features extracted from VITs. Regarding the CNN-derived features, our analysis reveals that *Energy*, and *TotalEnergy* emerge as the most prominently correlated features, with 15 correlations observed at a threshold of 0.3, 9 at 0.35, 4 at 0.4, and 2 at 0.45. Additionally, a high correlation (with $\rho = 0.45$) was established with *SizeZoneNonUniformity*, *DependenceNonUniformity*, and *RunLengthNonUniformity*. These 5 radiomic features (i.e. *Energy*, *TotalEnergy*, *SizeZoneNonUniformity*, *DependenceNonUniformity*, and *RunLengthNonUniformity*) collect all the correlations, both those with the original (unfiltered) version of the feature and those derived after filtering (considering the wavelets, with the 4 decompositions).

These correlations pave the way for pertinent clinical discussions, with implications already resonating within clinical practice. Further exploration of these clinical considerations is undertaken in Section 5.3.

5 Discussion

The concept of XAI is attracting much interest Holzinger et al. [2019], Stogiannos et al. [2023] and is playing a key role in the implementation and deployment of eXplainable Clinical Decision Support Systems (X-CDSSs). In this perspective, our work introduces several novelties. Rad4XCNN does not impose any methodological constraints that can harm the model performance to introduce explainability. In addition, it is agnostic, e.g. it is possible to apply it to

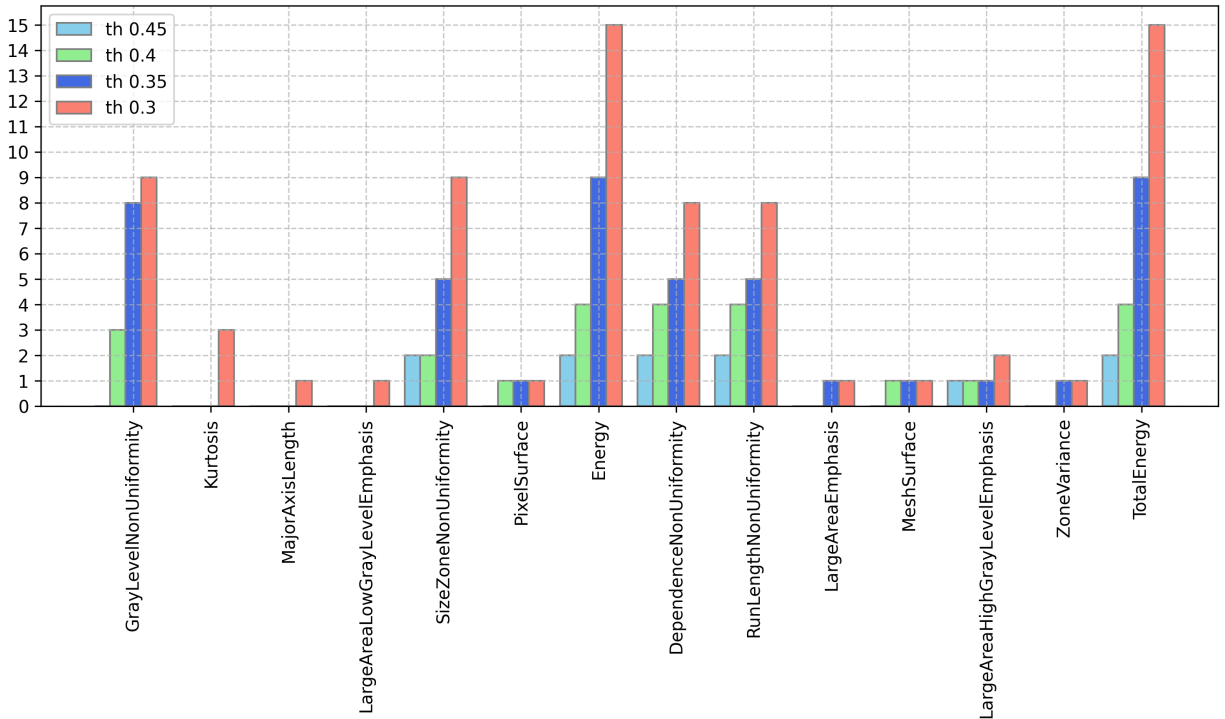


Figure 3: Global explanation of CNN-derived features obtained using Rad4XCNN. Each bar represents the number of CNN-derived features showing a correlation with radiomic features. The Y-axis reports the number of deep features correlated with the radiomic feature specified in the X-axis.

any CNN-based architecture. Our findings allowed us *i*) to find a substantial difference between radiomic, CNN-derived, and ViT-derived features, in terms of accuracy and explainability; *ii*) to analyze some concerns related to the field of XAI, which our method attempts to mitigate; *iii*) to highlight important clinical aspects in the context of breast cancer that are consistent with the clinical literature.

5.1 Comparing ViT-derived, CNN-derived and Radiomic Features

Rad4XCNN enabled an analysis of the role of radiomic, CNN-derived, and ViT-derived features, in terms of accuracy, explainability, and intrinsic meaning of deep features.

In terms of performance The ability of deep architectures to extract high and low level features makes deep features much more informative than radiomic ones. As a consequence, many works have shown that approaches exploiting deep features achieve higher performance than radiomics Lisson et al. [2022], Sun et al. [2020], Truhn et al. [2019], Wei [2021]. Hence, considering the evaluation on the external test, CNN-derived features enabled higher accuracy compared with ViT-derived. Regardless of datasets, ResNet maintains high accuracy values.

In terms of explainability Saliency maps generated through methods like GradCAM, EigenCAM, and ScoreCAM can effectively emphasize meaningful areas for prediction. While they serve as valuable visual and qualitative aids for prediction analysis, they present two primary concerns: *i*) each method yields distinct explanations, indicating a need for cautious interpretation; *ii*) these methods can lead to inter-operator variability evaluation, as individual physicians may interpret the explanations differently; *iii*) these explanations are inherently local, posing challenges for clinical validation of the models. In contrast, radiomic features offer clearer and more comparable explanations. Since it is possible to associate each radiomic feature with meaning/behavior related to its analytical definition, they enable the comparison of features identified in other studies with those observed in clinical practice, thereby enhancing their utility and reducing ambiguity.

Comparing CNN-derived and ViT-derived features As highlighted in Section 4.3, a notable alignment was observed between features derived from convolutional networks, whereas none was found with those extracted from ViT. This outcome aligns intuitively with an examination of the internal structures of the two architectures. CNN-based approaches typically rely on hierarchical feature extraction through a series of convolutional and pooling layers, capturing local patterns and spatial dependencies within the image. In contrast, ViT architectures adopt a self-attention mechanism, enabling them to capture global context by considering relationships between all image patches simultaneously. This leads CNNs to excel at capturing fine-grained details and local structures while ViTs in modeling long-range dependencies and contextual understanding. The authors themselves acknowledge that Transformers lack certain inherent biases found in convolutional neural networks, such as translation equivariance and locality [Dosovitskiy et al. [2020]]. This similarity between radiomic features and CNN-derived features arises from their shared principle of extracting local characteristics. Convolutional filters in CNNs capture local information through the Receptive Field kernels and a hierarchical structure of layers. Likewise, radiomic features are predominantly derived from matrices that analyze the relationships among gray levels of adjacent pixels. This common approach aligns CNN-derived features closely with radiomic features, setting them apart from ViT-derived features. For these reasons, Rad4XCNN is a global explanation method for CNN-derived features.

5.2 Mitigating XAI Concerns Through Rad4XCNN

Explainable AI is a challenging branch that certainly provides substantial advantages over traditional AI-based approaches for X-CDSS development and implementation. However, although there has been a tendency to integrate global and local model explanations into the conventional development pipeline, XAI has also raised some criticisms. In fact, it seems that in some circumstances, an explanation may have also negative effects: *i*) if the model displays less information, then excluding an explanation, users are not confused about the model (lower cognitive overload); *ii*) often, intrinsic explainability is weak, and users should be trained to understand the explanations; *iii*) it appears that end-users are more interested to understand *'what the system does'* rather than *'how the system works'* [Bell et al. [2022]]. However, some of the mentioned issues can be mitigated considering Rad4XCNN and are discussed below.

An Explanation Makes the Model Reliable? In our research, we uncovered a significant inconsistency in methods relying on saliency maps, a finding corroborated by numerous other studies [Cerekci et al. [2024], Prinzi et al. [2024a], Zhang et al. [2021]]. Consequently, even though these methods can identify where a model focuses for prediction, their reliability remains doubtful [Cerekci et al. [2024], Oh et al. [2020], Prinzi et al. [2023a, 2024a], Signoroni et al. [2021], Zhang et al. [2021]]. As a result, it is impossible to state with certainty the reliability of the trained model and to extract certain clinical insights.

In contrast, Rad4XCNN presents a novel approach distinct from visualization map-based methods, which is a new challenge in the realm of explainable methods in medical image analysis [Papanastasiou et al. [2023]]. This approach allows medical professionals to analyze whether radiomic features, whose significance is well defined, are in line with the clinical literature. In addition, it is possible to extract new clinical findings, such as those discussed in Section 5.3. This aspect overcomes the human tendency towards a positive interpretation of results by choosing the solution they want to be the correct one [Bornstein [2016]], providing an objective explanation.

Accuracy and Explainability trade-off Dilemma Achieving the trade-off between explainability and accuracy is still an open dilemma [Bell et al. [2022]]. Although this trade-off has been widely discussed, there are some experiments where it is highlighted that in the clinical context, a patient would prefer an accurate model rather than an explainable one [van der Veer et al. [2021]]. This would suggest that one should never sacrifice accuracy for the sake of explainability. Considering the absence of a definitive solution to this question, Rad4XCNN refrains from imposing constraints on model training. Instead, it provides an approach where radiomic features, although less predictive than deep ones, are exclusively utilized for explanatory purposes. It remains a task of the deep model to perform prediction accurately.

Explaining apparently incomprehensible patterns The abstraction mechanism within convolutional networks implies that the extracted features have a significantly higher level of abstraction than radiomic features. In this perspective, XAI methodologies must recognize that although it is possible to explain model decisions, understanding the relationships identified by deep architectures may be inherently incomprehensible. However, Rad4XCNN elucidates that a correlation exists between CNN-derived and radiomic features, demonstrating a convergence between physician insights and AI-based interpretations, as highlighted in the following section.

5.3 Radiomics-based explanation and its clinical validation

Rad4XCNN identified the radiomic features that exhibit the highest correlation with CNN-derived features, enabling us to draw significant clinical conclusions. Many of the radiomic features we discuss have already been used in previous studies, both diagnostic and prognostic, on the US radiomic analysis of focal breast lesions. For example, in the study by Cui *et al.* [2023] on the link between US radiomic features and biological functions in the prediction of HER2 status in breast cancer, Size Zone Non-Uniformity (SZNU) feature was associated with 1,871 genes in 75 perturbations and with carbon metabolism in cancer regarding biological functions; another radiomic feature analyzed in the same study Cui *et al.* [2023] was Run Length Non-Uniformity (RLNU), associated with the cell cycle and intercellular communication. In the study by Youk *et al.* on the analysis of the US radiomic features in benign and malignant breast masses Youk *et al.* [2020], 22 grayscale radiomic features were selected, some of which are also used in our study, such as Kurtosis, Energy, Run Length non-uniformity. Other radiomic features, although not yet applied to US image analysis, have already been analyzed in Prinzi *et al.* on breast cancer classification in DCE-MRI sequences Prinzi *et al.* [2024c]. The main results concerned features closely related to the intensity of grey levels: Energy and Total Energy. These radiomic features describe the change in grey intensity after administration of contrast medium, which is more rapid in malignant lesions, so these latter shows a more rapid increase in energy, *viceversa* for benign lesions. In breast US evaluation, excluding completely anechoic lesions, grey levels related to the echogenicity of a focal lesion may vary, but most malignant lesions are hypoechoic Rahbar *et al.* [1999]. Although the correlation between grey level intensity and the malignant lesion is different in DCE-MRI than in ultrasonographic features, even in ultrasonographic radiomic analysis, we can assert that both Energy and Total Energy emerge as characterizing features in ultrasonography, thereby laying a solid foundation for subsequent clinical investigations. The significance of signal intensity in US has been demonstrated in various anatomical districts Papini *et al.* [2002], Tessler *et al.* [2017], indicating its potential importance for breast imaging as well.

6 Conclusion

In this study, we have presented Rad4XCNN, a novel approach for the development of eXplainable Clinical Decision Support Systems, bridging the gap between accuracy and explainability without imposing methodological constraints on model performance. Through a comprehensive analysis comparing radiomic, Convolutional Neural Network (CNN)-derived, and Vision Transformer (ViT)-derived features in the context of breast cancer diagnosis, we have shed light on several critical aspects of XAI and its application in clinical decision-making.

Our findings highlight significant differences between radiomic, CNN-derived, and ViT-derived features in terms of accuracy and explainability. While deep architectures, particularly CNNs, demonstrate superior performance in terms of accuracy, radiomic features offer clearer and more comparable explanations due to their well-defined significance. Rad4XCNN revealed a notable alignment between CNN-derived and radiomic features, indicating shared principles of extracting local characteristics. Moreover, we addressed concerns surrounding XAI through (Rad4XCNN), offering insights into its reliability, the accuracy-explainability trade-off dilemma, and the complexity of deep model explanations. By identifying radiomic features that exhibit a high correlation with CNN-derived features we were able to draw some important clinical conclusions. The correlation between these features and those observed in previous studies on breast cancer diagnosis underscores the clinical relevance and potential utility of our findings.

In conclusion, the use of Radiomics in CNN explanation represents a promising advancement in the development of XCDSSs. It provides a new perspective on XAI methods that deviate from the methods based on visualization maps. In addition, it provides a form of global explanation, an aspect often overlooked in current research on explainable methods in medical imaging.

CRedit authorship contribution statement

Francesco Prinzi: conceptualization, methodology, software, formal analysis, writing original draft, visualization; **Carmelo Militello:** conceptualization, methodology, formal analysis, writing original draft, visualization; **Calogero Zarcaro:** validation, investigation, data curation; **Tommaso Vincenzo Bartolotta:** validation, investigation, data curation, supervision; **Salvatore Gaglio:** validation, investigation, writing - review and editing, supervision; **Salvatore Vitabile:** validation, investigation, resources, writing - review and editing, supervision, project administration, funding acquisition.

Funding

This research was co-funded by the Italian Complementary National Plan PNC-I.1 "Research initiatives for innovative technologies and pathways in the health and welfare sector" D.D. 931 of 06/06/2022, "DARE - DigitAI lifelong pRevEntion" initiative, code PNC0000002, CUP: B53C22006460001; and Finanziato dall'Unione europea – Next Generation EU - Progetti di Ricerca di Rilevante Interesse Nazionale (PRIN) 2022, Prot. 2022ENK9LS. Project: "EXEGETE: Explainable Generative Deep Learning Methods for Medical Image and Signal Processing", CUP: B53D23013040006.

Acknowledgments

The authors would like to thank Dr. Alice Latino for their substantial contribution to some experiments.

References

- Shinjini Kundu. Ai in medicine must be explainable. *Nature medicine*, 27(8):1328–1328, 2021. doi:10.1038/s41591-021-01461-z.
- Alejandro Barredo Arrieta, Natalia Díaz-Rodríguez, Javier Del Ser, Adrien Bennetot, Siham Tabik, Alberto Barbado, Salvador García, Sergio Gil-López, Daniel Molina, Richard Benjamins, et al. Explainable artificial intelligence (xai): Concepts, taxonomies, opportunities and challenges toward responsible ai. *Information fusion*, 58:82–115, 2020. doi:10.1016/j.inffus.2019.12.012.
- Andrew Smith and F Director. Using artificial intelligence and algorithms. *FTC*, Apr, 2020.
- Riccardo Guidotti, Anna Monreale, Salvatore Ruggieri, Franco Turini, Fosca Giannotti, and Dino Pedreschi. A survey of methods for explaining black box models. *ACM computing surveys (CSUR)*, 51(5):1–42, 2018. doi:10.1145/3236009.
- Julia Amann, Alessandro Blasimme, Effy Vayena, Dietmar Frey, Vince I Madai, and Precise4Q Consortium. Explainability for artificial intelligence in healthcare: a multidisciplinary perspective. *BMC medical informatics and decision making*, 20:1–9, 2020. doi:10.1186/s12911-020-01332-6.
- Carlo Combi, Beatrice Amico, Riccardo Bellazzi, Andreas Holzinger, Jason H Moore, Marinka Zitnik, and John H Holmes. A manifesto on explainability for artificial intelligence in medicine. *Artificial Intelligence in Medicine*, 133: 102423, 2022. doi:10.1016/j.artmed.2022.102423.
- Andreas Holzinger. Interactive machine learning for health informatics: when do we need the human-in-the-loop? *Brain Informatics*, 3(2):119–131, 2016. doi:10.1007/s40708-016-0042-6.
- Andreas Holzinger, Georg Langs, Helmut Denk, Kurt Zatloukal, and Heimo Müller. Causability and explainability of artificial intelligence in medicine. *Wiley Interdisciplinary Reviews: Data Mining and Knowledge Discovery*, 9(4): e1312, 2019. doi:10.1002/widm.1312.
- Aaron M Bornstein. Is artificial intelligence permanently inscrutable. *Nautilus*, 40, 2016.
- Marzyeh Ghassemi, Luke Oakden-Rayner, and Andrew L Beam. The false hope of current approaches to explainable artificial intelligence in health care. *The Lancet Digital Health*, 3(11):e745–e750, 2021. doi:10.1016/S2589-7500(21)00208-9.
- Liam G McCoy, Connor TA Brenna, Stacy S Chen, Karina Vold, and Sunit Das. Believing in black boxes: machine learning for healthcare does not need explainability to be evidence-based. *Journal of clinical epidemiology*, 142: 252–257, 2022. doi:10.1016/j.jclinepi.2021.11.001.
- Alex John London. Artificial intelligence and black-box medical decisions: accuracy versus explainability. *Hastings Center Report*, 49(1):15–21, 2019. doi:10.1002/hast.973.
- Mlađan Jovanović and Mia Schmitz. Explainability as a user requirement for artificial intelligence systems. *Computer*, 55(2):90–94, 2022. doi:10.1109/MC.2021.3127753.
- Esma Aktufan Cerekci, Deniz Alis, Nurper Denizoglu, Ozden Camurdan, Mustafa Ege Seker, Caner Ozer, Muhammed Yusuf Hansu, Toygar Tanyel, Ilkay Oksuz, and Ercan Karaarslan. Quantitative evaluation of saliency-based explainable artificial intelligence (xai) methods in deep learning-based mammogram analysis. *European Journal of Radiology*, page 111356, 2024.
- Francesco Prinzi, Marco Insalaco, Alessia Orlando, Salvatore Gaglio, and Salvatore Vitabile. A yolo-based model for breast cancer detection in mammograms. *Cognitive Computation*, 16(1):107–120, 2024a.

- Jiajin Zhang, Hanqing Chao, Mannudeep K Kalra, Ge Wang, and Pingkun Yan. Overlooked trustworthiness of explainability in medical ai. *medRxiv*, pages 2021–12, 2021.
- Robert J Gillies, Paul E Kinahan, and Hedvig Hricak. Radiomics: images are more than pictures, they are data. *Radiology*, 278(2):563–577, 2016. doi:10.1148/radiol.2015151169.
- Philippe Lambin, Ralph TH Leijenaar, Timo M Deist, Jurgen Peerlings, Evelyn EC De Jong, Janita Van Timmeren, Sebastian Sanduleanu, Ruben THM Larue, Aniek JG Even, Arthur Jochems, et al. Radiomics: the bridge between medical imaging and personalized medicine. *Nature reviews Clinical oncology*, 14(12):749–762, 2017. doi:10.1038/nrclinonc.2017.141.
- Francesco Prinzi, Alessia Orlando, Salvatore Gaglio, and Salvatore Vitabile. Interpretable radiomic signature for breast microcalcification detection and classification. *Journal of Imaging Informatics in Medicine*, 2024b. doi:10.1007/s10278-024-01012-1.
- Francesco Prinzi, Alessia Orlando, Salvatore Gaglio, and Salvatore Vitabile. Breast cancer classification through multivariate radiomic time series analysis in dce-mri sequences. *Expert Systems with Applications*, 249:123557, 2024c. doi:10.1016/j.eswa.2024.123557.
- Catharina Silvia Lisson, Christoph Gerhard Lisson, Marc Fabian Mezger, Daniel Wolf, Stefan Andreas Schmidt, Wolfgang M Thaiss, Eugen Tausch, Ambros J Beer, Stephan Stilgenbauer, Meinrad Beer, et al. Deep neural networks and machine learning radiomics modelling for prediction of relapse in mantle cell lymphoma. *Cancers*, 14(8):2008, 2022. doi:10.3390/cancers14082008.
- Qiuchang Sun, Xiaona Lin, Yuanshen Zhao, Ling Li, Kai Yan, Dong Liang, Desheng Sun, and Zhi-Cheng Li. Deep learning vs. radiomics for predicting axillary lymph node metastasis of breast cancer using ultrasound images: don't forget the peritumoral region. *Frontiers in oncology*, 10:53, 2020. doi:10.3389/fonc.2020.00053.
- Daniel Truhn, Simone Schradang, Christoph Haaburger, Hannah Schneider, Dorit Merhof, and Christiane Kuhl. Radiomic versus convolutional neural networks analysis for classification of contrast-enhancing lesions at multiparametric breast mri. *Radiology*, 290(2):290–297, 2019. doi:10.1148/radiol.2018181352.
- Peng Wei. Radiomics, deep learning and early diagnosis in oncology. *Emerging topics in life sciences*, 5(6):829–835, 2021. doi:10.1042/ETLS20210218.
- Giorgos Papanastasiou, Nikolaos Dikaios, Jiahao Huang, Chengjia Wang, and Guang Yang. Is attention all you need in medical image analysis? a review. *IEEE Journal of Biomedical and Health Informatics*, 2023.
- Luca Longo, Mario Brcic, Federico Cabitza, Jaesik Choi, Roberto Confalonieri, Javier Del Ser, Riccardo Guidotti, Yoichi Hayashi, Francisco Herrera, Andreas Holzinger, et al. Explainable artificial intelligence (xai) 2.0: A manifesto of open challenges and interdisciplinary research directions. *Information Fusion*, page 102301, 2024.
- Laurent Itti, Christof Koch, and Ernst Niebur. A model of saliency-based visual attention for rapid scene analysis. *IEEE Transactions on pattern analysis and machine intelligence*, 20(11):1254–1259, 1998. doi:10.1109/34.730558.
- Michail Mamalakis, Heloise de Vareilles, Atheer AI-Manea, Samantha C Mitchell, Ingrid Arartz, Lynn Egeland Morch-Johnsen, Jane Garrison, Jon Simons, Pietro Lio, John Suckling, et al. A 3d explainability framework to uncover learning patterns and crucial sub-regions in variable sulci recognition. *arXiv preprint arXiv:2309.00903*, 2023.
- Karen Simonyan, Andrea Vedaldi, and Andrew Zisserman. Deep inside convolutional networks: Visualising image classification models and saliency maps. *arXiv preprint arXiv:1312.6034*, 2013. doi:10.48550/arXiv.1312.6034.
- Mukund Sundararajan, Ankur Taly, and Qiqi Yan. Axiomatic attribution for deep networks. In *International conference on machine learning*, pages 3319–3328. PMLR, 2017.
- Matthew D Zeiler, Graham W Taylor, and Rob Fergus. Adaptive deconvolutional networks for mid and high level feature learning. In *2011 international conference on computer vision*, pages 2018–2025. IEEE, 2011. doi:10.1109/ICCV.2011.6126474.
- Matthew D Zeiler and Rob Fergus. Visualizing and understanding convolutional networks. In *Computer Vision–ECCV 2014: 13th European Conference, Zurich, Switzerland, September 6–12, 2014, Proceedings, Part I 13*, pages 818–833. Springer, 2014. doi:10.1007/978-3-319-10590-1_53.
- Jost Tobias Springenberg, Alexey Dosovitskiy, Thomas Brox, and Martin Riedmiller. Striving for simplicity: The all convolutional net. *arXiv preprint arXiv:1412.6806*, 2014. doi:10.48550/arXiv.1412.6806.
- Bolei Zhou, Aditya Khosla, Agata Lapedriza, Aude Oliva, and Antonio Torralba. Learning deep features for discriminative localization. In *Proceedings of the IEEE conference on computer vision and pattern recognition*, pages 2921–2929, 2016.

- Ramprasaath R Selvaraju, Michael Cogswell, Abhishek Das, Ramakrishna Vedantam, Devi Parikh, and Dhruv Batra. Grad-cam: Visual explanations from deep networks via gradient-based localization. In *Proceedings of the IEEE international conference on computer vision*, pages 618–626, 2017.
- Mohammed Bany Muhammad and Mohammed Yeasin. Eigen-cam: Class activation map using principal components. In *2020 international joint conference on neural networks (IJCNN)*, pages 1–7. IEEE, 2020.
- Francesco Prinzi, Carmelo Militello, Nicola Scichilone, Salvatore Gaglio, and Salvatore Vitabile. Explainable machine-learning models for COVID-19 prognosis prediction using clinical, laboratory and radiomic features. *IEEE Access*, 11:121492–121510, 2023a. doi:10.1109/ACCESS.2023.3327808.
- Yujin Oh, Sangjoon Park, and Jong Chul Ye. Deep learning covid-19 features on cxr using limited training data sets. *IEEE transactions on medical imaging*, 39(8):2688–2700, 2020.
- Alberto Signoroni, Mattia Savardi, Sergio Benini, Nicola Adami, Riccardo Leonardi, Paolo Gibellini, Filippo Vaccher, Marco Ravanelli, Andrea Borghesi, Roberto Maroldi, et al. Bs-net: Learning covid-19 pneumonia severity on a large chest x-ray dataset. *Medical Image Analysis*, 71:102046, 2021.
- Carmelo Militello, Francesco Prinzi, Giulia Sollami, Leonardo Rundo, Ludovico La Grutta, and Salvatore Vitabile. Ct radiomic features and clinical biomarkers for predicting coronary artery disease. *Cognitive Computation*, 15(1): 238–253, 2023. doi:10.1007/s12559-023-10118-7.
- Cynthia Rudin. Stop explaining black box machine learning models for high stakes decisions and use interpretable models instead. *Nature machine intelligence*, 1(5):206–215, 2019. doi:10.1038/s42256-019-0048-x.
- Haomin Chen, Catalina Gomez, Chien-Ming Huang, and Mathias Unberath. Explainable medical imaging ai needs human-centered design: guidelines and evidence from a systematic review. *npj Digital Medicine*, 5(1):156, 2022. doi:10.1038/s41746-022-00699-2.
- Rahul Paul, Matthew Schabath, Yoganand Balagurunathan, Ying Liu, Qian Li, Robert Gillies, Lawrence O Hall, and Dmitry B Goldgof. Explaining deep features using radiologist-defined semantic features and traditional quantitative features. *Tomography*, 5(1):192–200, 2019.
- Clinton J Wang, Charlie A Hamm, Lynn J Savic, Marc Ferrante, Isabel Schobert, Todd Schlachter, MingDe Lin, Jeffrey C Weinreb, James S Duncan, Julius Chapiro, et al. Deep learning for liver tumor diagnosis part ii: convolutional neural network interpretation using radiologic imaging features. *European radiology*, 29:3348–3357, 2019.
- Sihong Chen, Jing Qin, Xing Ji, Baiying Lei, Tianfu Wang, Dong Ni, and Jie-Zhi Cheng. Automatic scoring of multiple semantic attributes with multi-task feature leverage: a study on pulmonary nodules in ct images. *IEEE transactions on medical imaging*, 36(3):802–814, 2016.
- Alex Zwanenburg, Martin Vallières, Mahmoud A Abdalah, Hugo JWL Aerts, Vincent Andrearczyk, Aditya Apte, Saeed Ashrafinia, Spyridon Bakas, Roelof J Beukinga, Ronald Boellaard, et al. The image biomarker standardization initiative: standardized quantitative radiomics for high-throughput image-based phenotyping. *Radiology*, 295(2): 328–338, 2020. doi:10.1148/radiol.2020191145.
- Caixia Liu, Ruibin Zhao, and Mingyong Pang. Semantic characteristic grading of pulmonary nodules based on deep neural networks. *BMC Medical Imaging*, 23(1):156, 2023.
- Walid Al-Dhabyani, Mohammed Gomaa, Hussien Khaled, and Aly Fahmy. Dataset of breast ultrasound images. *Data in brief*, 28:104863, 2020. doi:10.1016/j.dib.2019.104863.
- Edward A Sickles and Carl J D’Orsi. How should screening breast US be audited? the BI-RADS perspective. *Radiology*, 272(2):316–320, 2014. doi:10.1148/radiol.14140634.
- Anna Pawłowska, Piotr Karwat, and Norbert Żółek. Letter to the editor. re: “[dataset of breast ultrasound images by w. al-dhabyani, m. gomaa, h. khaled & a. fahmy, data in brief, 2020, 28, 104863]”. *Data in Brief*, 48:109247, 2023. ISSN 2352-3409. doi:10.1016/j.dib.2023.109247.
- Haofan Wang, Zifan Wang, Mengnan Du, Fan Yang, Zijian Zhang, Sirui Ding, Piotr Mardziel, and Xia Hu. Score-cam: Score-weighted visual explanations for convolutional neural networks. In *Proceedings of the IEEE/CVF conference on computer vision and pattern recognition workshops*, pages 24–25, 2020.
- Joost JM Van Griethuysen, Andriy Fedorov, Chintan Parmar, Ahmed Hosny, Nicole Aucoin, Vivek Narayan, Regina GH Beets-Tan, Jean-Christophe Fillion-Robin, Steve Pieper, and Hugo JWL Aerts. Computational radiomics system to decode the radiographic phenotype. *Cancer research*, 77(21):e104–e107, 2017. doi:10.1158/0008-5472.CAN-17-0339.
- Francesco Prinzi, Carmelo Militello, Vincenzo Conti, and Salvatore Vitabile. Impact of wavelet kernels on predictive capability of radiomic features: A case study on COVID-19 chest X-ray images. *Journal of Imaging*, 9(2):32, 2023b. doi:10.3390/jimaging9020032.

- Carmelo Militello, Leonardo Rundo, Mariangela Dimarco, Alessia Orlando, Ildebrando D'Angelo, Vincenzo Conti, and Tommaso Vincenzo Bartolotta. Robustness analysis of DCE-MRI-derived radiomic features in breast masses: Assessing quantization levels and segmentation agreement. *Applied Sciences*, 12(11):5512, 2022. doi:10.3390/app12115512.
- Nikolaos Papanikolaou, Celso Matos, and Dow Mu Koh. How to develop a meaningful radiomic signature for clinical use in oncologic patients. *Cancer Imaging*, 20:1–10, 2020. doi:10.1186/s40644-020-00311-4.
- Francesco Prinzi, Alessia Orlando, Salvatore Gaglio, Massimo Midiri, and Salvatore Vitabile. ML-Based radiomics analysis for breast cancer classification in DCE-MRI. In Mufti Mahmud, Cosimo Ieracitano, M. Shamim Kaiser, Nadia Mammone, and Francesco Carlo Morabito, editors, *Applied Intelligence and Informatics*, pages 144–158. Springer Nature Switzerland, 2022. doi:10.1007/978-3-031-24801-6_11.
- N Stogiannos, H Bougias, E Georgiadou, S Leandrou, and P Papavasileiou. Analysis of radiomic features derived from post-contrast t1-weighted images and apparent diffusion coefficient (adc) maps for breast lesion evaluation: A retrospective study. *Radiography*, 29(2):355–361, 2023. doi:10.1016/j.radi.2023.01.019.
- Alexey Dosovitskiy, Lucas Beyer, Alexander Kolesnikov, Dirk Weissenborn, Xiaohua Zhai, Thomas Unterthiner, Mostafa Dehghani, Matthias Minderer, Georg Heigold, Sylvain Gelly, et al. An image is worth 16x16 words: Transformers for image recognition at scale. *arXiv preprint arXiv:2010.11929*, 2020.
- Andrew Bell, Ian Solano-Kamaiko, Oded Nov, and Julia Stoyanovich. It's just not that simple: an empirical study of the accuracy-explainability trade-off in machine learning for public policy. In *2022 ACM Conference on Fairness, Accountability, and Transparency*, pages 248–266, 2022. doi:10.1145/3531146.3533090.
- Sabine N van der Veer, Lisa Riste, Sudeh Cheraghi-Sohi, Denham L Phipps, Mary P Tully, Kyle Bozentko, Sarah Atwood, Alex Hubbard, Carl Wiper, Malcolm Oswald, et al. Trading off accuracy and explainability in ai decision-making: findings from 2 citizens' juries. *Journal of the American Medical Informatics Association*, 28(10):2128–2138, 2021. doi:10.1093/jamia/ocab127.
- Hao Cui, Yue Sun, Dantong Zhao, Xudong Zhang, Hanqing Kong, Nana Hu, Panting Wang, Xiaoxuan Zuo, Wei Fan, Yuan Yao, et al. Radiogenomic analysis of prediction her2 status in breast cancer by linking ultrasound radiomic feature module with biological functions. *Journal of Translational Medicine*, 21(1):44, 2023.
- Ji Hyun Youk, Jin Young Kwak, Eunjung Lee, Eun Ju Son, and Jeong-Ah Kim. Grayscale ultrasound radiomic features and shear-wave elastography radiomic features in benign and malignant breast masses. *Ultraschall in der Medizin-European Journal of Ultrasound*, 41(04):390–396, 2020.
- Guita Rahbar, Angela C Sie, Gail C Hansen, Jeffrey S Prince, Michelle L Melany, Handel E Reynolds, Valerie P Jackson, James W Sayre, and Lawrence W Bassett. Benign versus malignant solid breast masses: Us differentiation. *Radiology*, 213(3):889–894, 1999.
- Enrico Papini, Rinaldo Guglielmi, Antonio Bianchini, Anna Crescenzi, Silvia Taccogna, Francesco Nardi, Claudio Panunzi, Roberta Rinaldi, Vincenzo Toscano, and Claudio M Pacella. Risk of malignancy in nonpalpable thyroid nodules: predictive value of ultrasound and color-doppler features. *The Journal of Clinical Endocrinology & Metabolism*, 87(5):1941–1946, 2002.
- Franklin N Tessler, William D Middleton, Edward G Grant, Jenny K Hoang, Lincoln L Berland, Sharlene A Teefey, John J Cronan, Michael D Beland, Terry S Desser, Mary C Frates, et al. Acr thyroid imaging, reporting and data system (ti-rads): white paper of the acr ti-rads committee. *Journal of the American college of radiology*, 14(5): 587–595, 2017.